EDGE BEARING TESTS TO ASSESS THE INFLUENCE OF RADIAL GRADATION ON THE TRANSVERSE BEHAVIOR OF BAMBOO

Richard Moran[a], Kelly Webb[b], Kent Harries[c], José Jaime García[a]

[a] Escuela de Ingeniería Civil y Geomática, Universidad del Valle, Cali, Colombia;

[b] Department of Civil Engineering, Architecture and Building, Coventry University, United Kingdom;

[c] Department of Civil and Environmental Engineering, University of Pittsburgh, United States;

[a]richard.moran@correounivalle.edu.co, [b]webbk6@uni.coventry.ac.uk,[c]kharries@pitt.edu,

[a]josejgar@gmail.com,

ABSTRACT

Bamboo is a sustainable material with high potential for structural applications. The aim of this study was to use edge bearing tests, digital image correlation analysis, and finite element simulations to research about the distribution of the circumferential elastic modulus through the wall and the associated failure strain and stress. Studied bamboo species were *Phyllostachys edulis* (Moso), *Bambusa stenostachya* (Tre Gai) and *Guadua angustifolia* (Guadua). Using the edge bearing tests, the effective circumferential moduli under compression were similar to those obtained under tension. Mean effective moduli were 1358.5 MPa, 662 MPa, and 862 MPa for bamboo Moso, Tre Gai, and Guadua, respectively. Linear, exponential and parabolic functions that were proposed to represent the circumferential modulus provided a relatively good fitting of the experimental results. Due to the radial gradation, the circumferential moduli at the outer position were 2.3, 1.9, and 2.6 higher than those at the inner location for Moso, Tre Gai, and Guadua, respectively. Mean circumferential failure strains and stresses in the inner culm surface were: 6693 με and 7.6 MPa; 13137 με and 12.1 MPa; and 5948 με and 3.7 MPa for Moso, Tre Gai and Guadua respectively.

Key words: Bamboo, digital image correlation, finite element method, circumferential elastic modulus, functional graded material.

1. INTRODUCTION

Bamboo is a variety of giant grass widely available in tropical zones around the world [1]. Bamboo has shown great potential as a sustainable material, due to its fast growth and maturation, and its capacity to sequester CO_2 and regulate water cycles [2-3]. Furthermore, bamboo has excellent potential as a structural material because of his tubular shape and the fact that itsaxial strength is similar to that of low carbon steel [4-5].

Bamboo culms consist of hollow cylindrical internodes reinforced with transverse diaphragms dispersed along their length. The internodes behave mechanically as a hollow cylinder reinforced with axially oriented cellulose fibers embedded in a weak matrix of lignin [5]. Thus, mechanical properties are highly anisotropic, with large strength and stiffness in the axial direction and poor properties in the transverse directions [6-7]. In addition, bamboo is a heterogeneous material as the fiber density increases from the inner to the outer wall faces of the internode cross-section. For this reason, bamboo is often referred to as a functionally graded material [8-9].

Despite its attributes, the use of bamboo in construction remains limited primarily to 'non-engineered' or vernacular structural forms. This is due in part to the considerable dimensional and mechanical property variation among culms and even along the length of a single culm. In addition, due to the unidirectional fiber-reinforced structure of the material, longitudinal splitting is a typical failure mode in bamboo members [5, 10-12]. Splitting failures are often critical at structural joints, where high localized shear and tensile circumferential stresses are generated, due for example to the presence of holes in bolted connections [12]. The splitting mode of failure is also present, and often is dominant, in bending [5] and even in compression.

One the main challenges in bamboo construction is the development of efficient connections, which are difficult to build due to the hollow cylindrical shape of the culms. In order to design efficient and inexpensive connections for bamboo members, an understanding of the failure modes and stress distribution in critical regions is necessary. However, this can only be achieved using constitutive models that can accurately capture the anisotropic and heterogeneous behavior of the material. In this regard, most experimental studies focus on axial property characterization [9, 13-16], while transverse properties remain poorly understood, even though most bamboo failures are initiated within the fiber planes due to the transverse components of the stress tensor.

Few studies have been carried out to determine transverse mechanical properties of bamboo. Torres et al. [17] proposed an edge bearing test and a transverse isotropic law to calculate the effective circumferential elastic modulus of *Phyllostachys edulis* (Moso) and *Guadua angustifolia* (Guadua) rings. Sharma et al.[10] tested thin-walled Moso and thick-walled *Bambusa stenostachya* (Tre Gai) rings using the edge bearing test to determine strain profiles and the effective circumferential elastic modulus. Circumferential strength results were compared with split-pin transverse tension tests in which a fracture mechanics approach was used to investigate the splitting failures [18]. However, no distribution of elastic modulus was proposed, and it was recognized that more research is necessary to determine the influence of fiber gradation through the culm wall thickness on the mechanical transverse behavior of bamboo.

Lee et al. [19] developed a test arrangement using bamboo rings under internal pressure. To analyze the variation of the circumferential elastic modulus through the culm wall thickness, linear, power and exponential distributions were used to fit the inner and outer strain measurements. Based on this study Lee et al. [19] proposed an exponential distribution for the circumferential modulus. Lee et al. [19] did not report the species used although a review of available literature [20] indicates that through-wall modulus distribution is species dependent.

Thus, the goal of this study was to investigate the variation of the circumferential Young's modulus of bamboo with radial position. The circumferential compression, or 'edge bearing' test was used together with digital image correlation (DIC) and finite element (FE) models to assess the distribution of circumferential elastic modulus of three bamboo species. Additionally, circumferential failure strains and stresses were determined.

2. METHODS

2.1 Material

Rings were extracted from internode zones of three species of bamboo: *Phyllostachys edulis* (Moso), *Bambusa stenostachya* (Tre Gai) and *Guadua angustifolia* Kunt (Guadua).

These are commercially viable species in China, Southeast Asia, and South America, respectively. All rings came from borax salt treated culms [6-7, 10]. Rings were extracted from four different culms of Tre Gai and Moso and five different culms of Guadua, although location along the culm of the rings was not available for any bamboo species. Specimens were labeled as X-YYZ, where the first letter (X) was used to identify the species (M for Moso, T for Tre Gai and G for Guadua), and the following three numbers were used to identify the culm number (YY) and the specimen number from the culm (Z).

Moisture content was measured in eight locations for every test specimen using a test probe (EXTECH Moisture Meter 0220), the average moisture values measured were: 12.4% (COV= 0.06) for Moso, 14.4% (COV = 0.17) for Tre Gai and 11.6% (COV = 0.05) for Guadua.

All rings were marked at four quadrants (N, E, S and W). Diameters (D) were measured across N-S and E-W positions, while thickness (t) and ring specimen length (L) were measured at each quadrant. Average dimensions of tested specimens for each species and load type (described subsequently) are reported in Table 1.

For the compression tests, L/D ring ratios were 0.59 (COV =0.09), 0.58 (COV =0.03), and 0.41 (COV =0.03) for Moso, Thre Gai, and Guadua, respectively. For the tension tests, L/D ratios were 0.48 (COV = 0.2), 0.15 (COV = 0.08), and 0.41 (COV = 0.05) for Moso, Thre Gai, and Guadua, respectively. A lower L/D ratio for the Thre Gai rings under tension was necessary to be able to test these thick-walled rings in the tension fixture described below.

2.2 Edge bearing test

The edge bearing or transverse compression test has been used to characterize transverse effective properties of bamboo rings [10, 17]. In this test, specimens are loaded across their diameter (load points are designated N and S) and the load and vertical or horizontal displacement (*Δv* or *Δh*) are recorded (Figure 1).

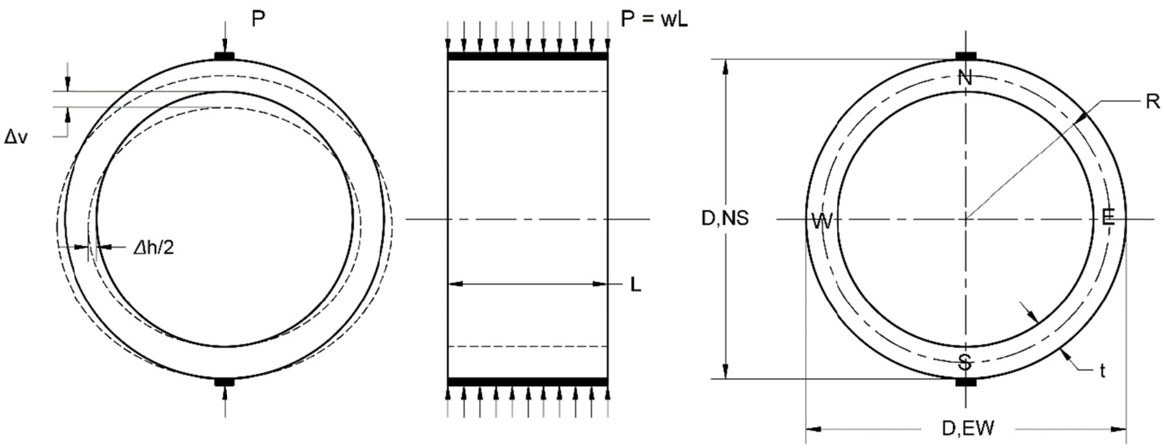

Figure 1. Edge *bearing* compression test and characteristic geometric dimensions

Under the assumption of the material as homogeneous and transverse isotropic, each displacement *Δv* or *Δh* of Figure 1 can be determined in terms of the load *P*, the effective circumferential elastic modulus E_{ϕ}, and the geometrical parameters of the ring by using the Castigliano´s theorem described in texts of solid mechanics [21]. These formulas are presented in [22]. As the vertical displacement *Δv* was measured in the compression experiment, the circumferential modulus was calculated as,

$$E_{\emptyset} = \frac{12PR^3}{Lt^3\Delta_v} * (\frac{\pi k_1}{4} - \frac{2{k_2}^2}{\pi}). \quad (1)$$

On the other hand, as the horizontal displacement Δ_h was measured in the tension experiment, the elastic modulus was calculated using,

$$E_{\emptyset} = \frac{12PR^3}{Lt^3\Delta_h} * \left(\frac{k_1}{2} - k_2 + \frac{2{k_2}^2}{\pi}\right). \tag{2}$$

Where k_1 and k_2 are correction factors equal to:

$$k_1 = \left(1 - \frac{t^2}{12R^2} + \frac{FEt^2}{12GR^2}\right), \text{ and} \tag{3}$$

$$k_2 = \left(1 - \frac{t^2}{12R^2}\right) \text{ for thin rings, and} \tag{4}$$

$$k_2 = \left(\frac{t}{Rln\frac{R_o}{R_i}}\right) \text{ for thick rings.} \tag{5}$$

In which R is the mean radius of the ring *(D/2 – t/2)*, R_o and R_i are inner and the outer radii, respectively, and t is the culm wall thickness. Finally, considering a transverse isotropic model the ratio E/G is assumed to be 2(1+ν), where the Poisson's ratio, ν= 0.22 [6] and the shape factor F = 1.2 for a rectangular section [10].For the purposes of understanding trends, k_2 may be estimated to be equal to 1 while $k_1 \approx 1+0.16t^2/R^2$ without introducing significant error.

In order to understand failures in the tests and strain measurements, stress and strain analysis can be carried out considering an isotropic and homogeneous material [22]. Assuming symmetry, the moments at the North and South quadrants are equal to:

$$M_{NS} = \frac{PRk_2}{\pi}\,. \tag{6}$$

Similarly, the East and West moments can be calculated as:

$$M_{EW} = \frac{PRk_2}{\pi} - \frac{PR}{2}, \tag{7}$$

Where P is total load applied uniformly over length L. Circumferential stresses in the corresponding quadrants are calculated as:

$$\sigma_{NS} = \frac{M_{NS}}{Lth}\frac{(R-r-h)}{r} \tag{8}$$

and,

$$\sigma_{EW} = \frac{M_{EW}}{Lth}\frac{(R-r-h)}{r} - \frac{P}{2Lt}, \tag{9}$$

where r, ranging from R_i to R_o, is the radial position where the stress is calculated and h defines the shift in position of the neutral axis in the curved culm wall segment from its centroid ($t/2$) when subject to flexure. For a rectangular cross section, h is given as:

$$h = R - \frac{t}{ln\left[\frac{2R+t}{2R-t}\right]} \ . \tag{10}$$

Sincek_2 is approximately equal to 1, the magnitudes of the N-S moments are about 75% greater than that of the E-W moments, hence failures in the N-S positions should dominate behavior. This, however, is not always the case since the gradient of material properties through the culm wall results in the shift in neutral axis toward the external surface of the ring which complicates behavior [10].Nevertheless, if the ring is loaded in tension (that is P is reversed in Figure 1), the superposition of the normal load and the bending moment in the East and West quadrants (Eq. 7) may lead to failure since the additional normal component of stress *(P/2Lt* in Eq. 9*)* is superposed in quadrants E-W. Therefore, at these positions, the neutral axis radial position R_{EW} in the culm wall is shifted further toward the external surface of the ring, as can be calculated from:

$$R_{EW} = \frac{2\,M_{NW\,(R-h)}}{2\,M_{NW} + hP} \ . \tag{11}$$

The normalized neutral axis position with respect to the interior surface of the culm wall for N-S and E-W quadrants can be calculated as:

$$N.A_{NS} = \frac{(R-h-R_i)}{t}, \text{ and} \quad (12)$$

$$N.A_{EW} = \frac{(R_{EW}-R_i)}{t} \quad (13)$$

One objective of the present study is to address the orientation of the load and its effect on test behavior. When tested in compression, the internal moments result in the inner culm wall at the N and S quadrants and the outer wall at E and W quadrants being placed in tension. When tested in tension, the opposite moment orientations result and the normal component of load at the E and W quadrants reverses (sign of P change in Eqs. 6, 7 and 9). This reversal, it was thought, may impact circumferential modulus measurements. Additionally, it was hypothesized that the local effects of the introduction of the load at the 'compression' face of the N and S quadrants may affect overall behavior at these quadrants meaning that only data from the E or W quadrant are valid. If this were the case, both compression and tension tests are required to fully investigate through-culm-wall properties.

2.3 Experimental setup

Compression tests were carried out using a precision gear-driven compression machine (Wykeham Farrance 5-Ton) with a 45 kN load cell having a resolution of 4.5 N. The load was applied at the N and S positions while the vertical displacement was measured with a linear position transducer (regal 9600-series) placed within the ring (Figure 2a). Neoprene pads 10 mm wide and 3.4 mm deep were used to distribute the loads evenly along the N and S lengths of the specimen. In order to measure displacements and strain profiles in the transverse cross-section of the ring, a VIC3D digital image correlation (DIC) system was used (Correlated Solutions Inc.). Before testing, all specimens were painted with a white base paint and sprayed with black matte paint to generate the speckle pattern required for the DIC cameras (Fig 2b). Load and displacement data were recorded at the same regular intervals at which DIC images were obtained. All the tests were carried out under displacement control at a speed of 0.019mm/s.

a. b.

Fig 2. Compression edge bearing test, a. Test arrangement (one DIC camera is in foreground), b. Bamboo rings prepared for DIC measurement.

2.3.1 Edge bearing tension test

To examine possible differences in the apparent transverse modulus associated with the direction of bending, a tension edge bearing test apparatus (Figure 3) was developed, allowing the tension test to be conducted in the same machine used for the compression tests. In this test, diametric tension was applied across the N-S diameter of the bamboo ring. In this case, load is applied to the inner wall of the ring at N and S and the ring is ‘pulled’ vertically. East and West strain profiles for the tension tests were also obtained using DIC (the test frame obscured the N and S locations). To facilitate the tension test setup, the horizontal internal displacement was measured instead the vertical (Figure 3b). Tension tests were conducted at the same applied displacement rate of 0.019 mm/s.

a. b.

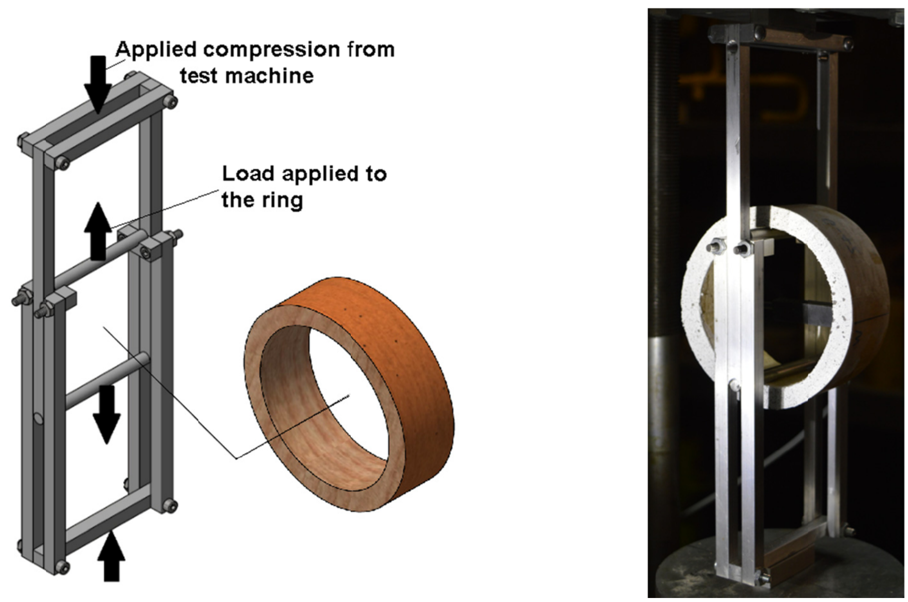

Figure 3. Tension edge bearing test. a. Tension apparatus, b. Test set up.

3. TEST RESULTS

As summarized in Table 1, 54 specimens were tested. Table 1summarizes the key experimental results from this test program; these are discussed further in subsequent sections.

Defects in specimens that appear in Table 1 were micro cracks that were only detected with the DIC measurements. However, these defects were not critical for the measured parameters, as confirmed by a statistical analysis (not presented in this paper) that showed no difference between results from defective and free-defect specimens.

Table 1. Summary ofspecimen geometry and test key results (COV in brackets)

Species	Loadtype	*n*	*D*	*t*	*L*	s_h or s_v	E_φ	Neutral axis location	Location of failures		Samples with defects
			mm	mm	mm	N/mm	MPa	mm/mm	NS	EW	
Moso	C	9	86.0 (0.10)	9.3 (0.09)	50.7 (0.04)	607 (0.62)	1355 (0.24)	0.59 (0.23)	4	5	6
	T	8	86.0 (0.10)	10.4 (0.21)	50.7 (0.04)	389 (0.25)	1362 (0.20)	0.53 (0.09)	8	0	2
Tre Gai	C	6	88.5 (0.06)	22.4 (0.12)	51.1 (0.01)	4109 (0.39)	766 (0.34)	0.67 (0.07)	6	0	2
	T	11	97.3 (0.04)	19.2 (0.42)	14.4 (0.06)	1622 (1.54)	558 (0.74)	0.68 (0.10)	11	0	0
Guadua	C	10	117.0 (0.02)	12.7 (0.22)	47.9 (0.02)	256 (0.11)	864 (0.31)	0.59 (0.16)	10	0	4
	T	10	116.7 (0.02)	12.8 (0.22)	47.4 (0.03)	341 (0.30)	860 (0.30)	0.59 (0.16)	7	4	4

3.1 Effective elastic properties

Load versus displacement curves exhibited an essentially linear behavior up to about 80% of the maximum load at failure for both the tension and compression tests (Figure 4). For all tests, the slopes of the force versus deflection curves were calculated using least square fitting of the data up to approximately 60% of the ultimate capacity. For compression, the slopes s_v were 607 N/mm, 4109N/mm and 256N/mm, for Moso, Tre Gai and Guadua, respectively. In the tension tests the slopes s_h were 389 N/mm, 1622 N/mm and 341 N/mm for Moso, Tre Gai and Guadua, respectively. The coefficient of determination, R^2, was greater than 0.99 in all cases indicating a very linear response.

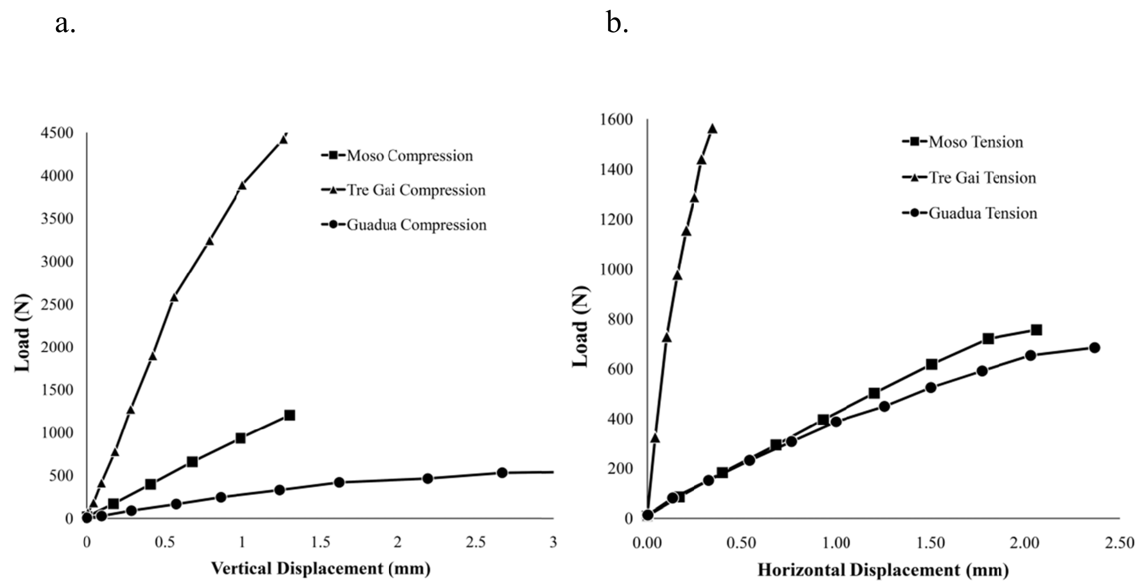

Figure 4. Typical loading curves, a. Compression, b. Tension.

In the compression tests, the circumferential elastic modulus, calculated using Eq. 1, of bamboo Moso was 76% and 56% greater than those of Tre Gai and Guadua, likewise in tension tests (Eq. 2) it was 143% and 58% greater than those of Tre Gai and Guadua, respectively. No statistical differences in $E_{\emptyset}$ determined from compression or tension tests were found for any species (Figure 5).

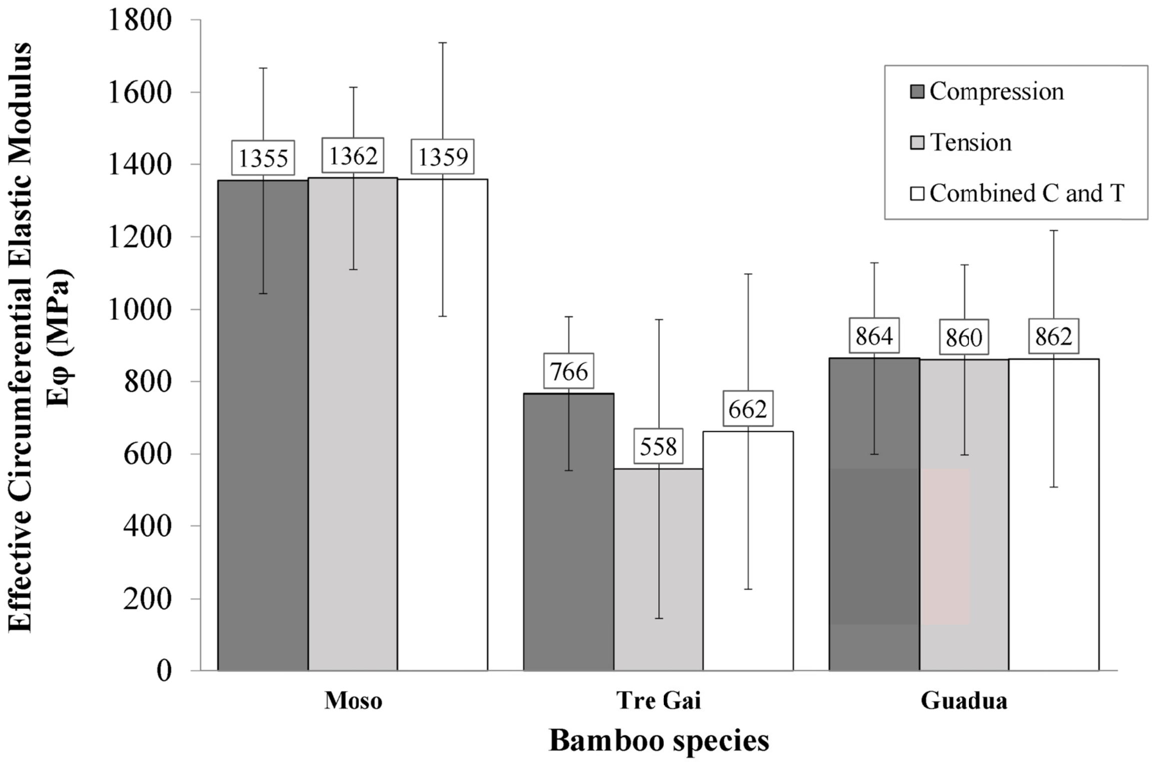

Figure 5. Effective elastic circumferential moduli determined from compression and tension tests. Error bars represent one standard deviation

3.2 Strain profiles

Circumferential strain – determined from DIC data such as that shown in Figure 6 – in the four quadrants of the rings exhibited nonlinear profiles (Figure 7), which were more pronounced for the thick Tre Gai rings.

a. b.

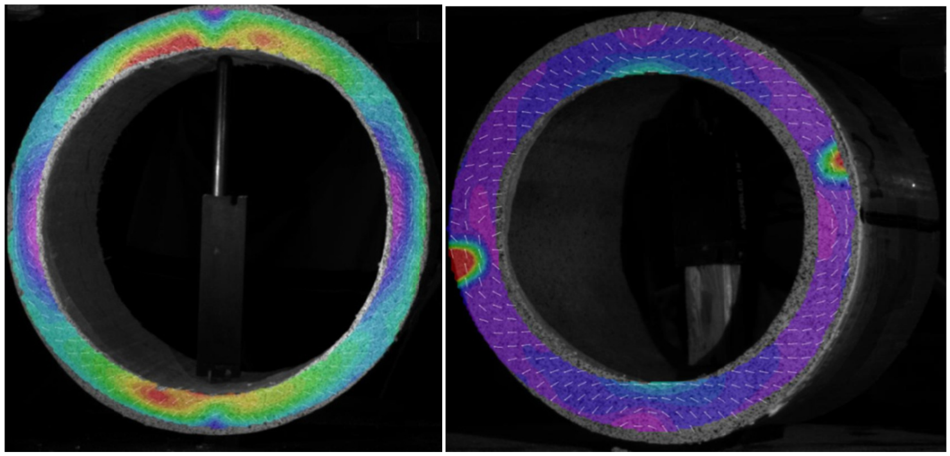

Figure 6. Profiles of the maximum principal strain, a. Relatively defect-free specimen (Guadua G-34), b. Specimen with preexistent cracks (Moso M-13).

a. b.

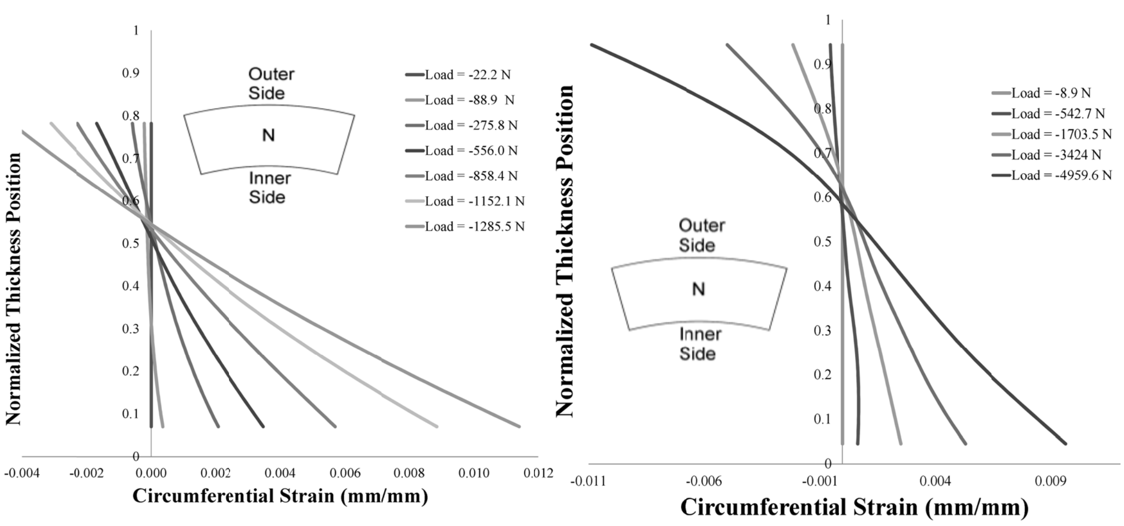

c.

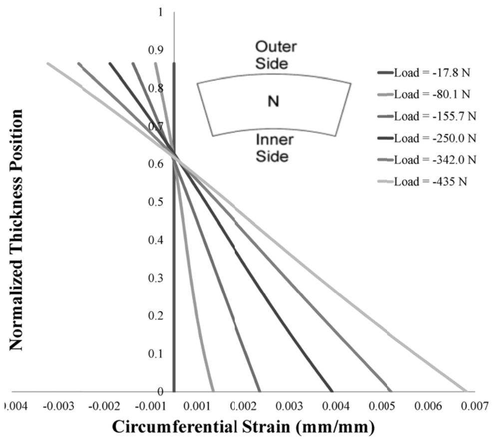

Figure 7. Experimental strain profiles in compression test (North position), a. Moso (M-13), b. Tre Gai(T-11) and c. Guadua (G-25).

The observed positions of the neutral axis, normalized to the wall thickness, relative to the interior culm wall were of 0.59, 0.68 and 0.59 for Moso, Tre Gai and Guadua, respectively (Figure 7). No statistical differences in the neutral axis position between compression and tension loading were found. The position of the neutral axis in the East and West quadrants calculated using Eq. 13assuming a homogeneous material and formulas valid for curved beams [21] were 0.53, 0.59 and 0.54 for Moso, Tre Gai and Guadua, respectively. The radial gradation of the material accounts for the larger observed values.

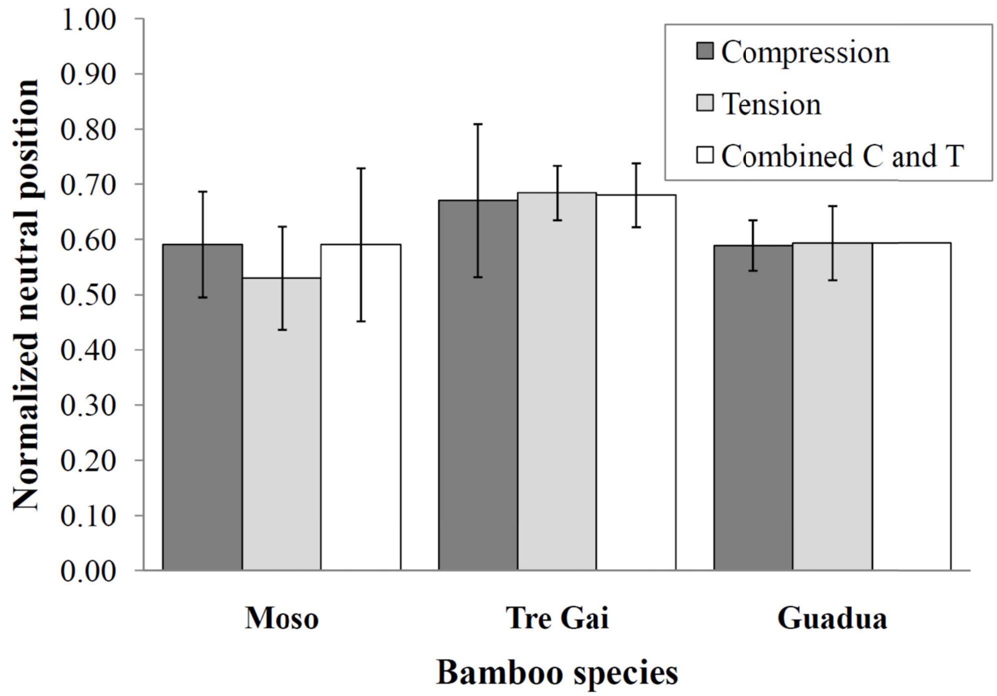

Figure 8. Normalized neutral axis position for all species under both loading conditions. Error bars represent one standard deviation

Even in a relatively defect-free specimen (Figure 6a), the strain profiles were not perfectly symmetric due to geometry variations of the rings. In specimens having an initial defect (Figure 6b, having existing longitudinal cracks), the strain concentrations are pronounced and affect the final failure of the test. The experimental strain at the N and S locations of the tension tests was not available since the test apparatus masked the specimen from the DIC camera.

3.3 Failures analysis

From the 54 specimens tested, 46 failed at the N-S positions (Table 1). Five Moso specimens failed at the E-W positions in the compression tests, while three Guadua specimens under tension failed at the E-W positions, which may be attributed to preexisting imperfections in some specimens. The typical failure in both, the compression and tension tests, occurred at the N-S locations with the tensile crack opening at the inner culm wall surface when tested in compression and at the outer surface when tested in tension.(Figure 9).

a. b. c.

Figure 9. Failure types.a. Under compression load (T-14), b. Under tension load (T-94), c. Failure due to preexisting crack (G-44).

Maximum tensile strains at failure were calculated for the compression specimens that crackedon the inner surface (Figure 9a). The tension failure strains determined from DIC were: 6693 $\mu\varepsilon$ (COV = 0.44), 13137 $\mu\varepsilon$ (COV = 0.26) and 5948 $\mu\varepsilon$ (COV = 0.39) for Moso, Tre Gai and Guadua, respectively.

3.4 Finite Element modeling and fitting

The formulas presented previously are based on homogeneous material properties through the culm wall. A finite element (FE) approach in which the distribution of circumferential modulus was varied in order to best match the experimentally observed loading curves and strain profiles was used to investigate the heterogeneous nature of the culm wall. All FE models were developed using ABAQUS (Simulia Corp.). Results from six ring models, two for each species, one in compression and the other in tension, were fitted to the experimentally responses. A three dimensional FE mesh was built with eight-node linear brick elements with reduced integration and hourglass control (ABAQUS element type C3D8R). The mesh size was selected after a convergence analysis with displacements differences less than 2% between successive meshes. Divisions smaller than 1 mm were prescribed through the thickness in order to obtain an accurate description of the change of E_φ and thus effectively model the functionally graded material (FGM). Defect-free defect rings were chosen and average dimensions were used to model the rings as perfect hollow cylinders.

Anisotropy and heterogeneity were considered. To be able to consider the anisotropy, the elastic properties were defined based on a cylindrical coordinate system, in which the r, θ and z axes were oriented in the radial, circumferential and axial directions of the culm, respectively. In order to account for the material gradation through the culm wall thickness, an artificial radial temperature field was prescribed and the transverse elastic properties were defined to be a function of this field. Regarding other material properties, a parametric analysis was conducted indicating that only E_ϕ and $G_{r\phi}$ have influence in the results, where E_ϕ has the dominant effect; therefore, just this parameter was fitted. Transverse isotropic behavior was assumed making $E_r = E_\phi$, $G_{r\phi} = E_\phi/(2(1+\nu_{r\phi}))$, with $\nu_{r\phi} = 0.22$ [6].All remaining anisotropic constants were kept constant as: E_z = 13420 MPa [23], $\nu_{rz} = \nu_{\phi z} = 0.01$ and G_{rz} = G_{rz} = 581 MPa [6].

The distribution of elastic modulus was fitted with linear, parabolic, and exponential functions, which have been used previously to describe bamboo gradation [15-16, 19]. These functions are:

Linear: $$E_\varphi(r) = m\left(\frac{r-R_0}{t}\right) + b, \quad (14a)$$

Parabolic: $$E_\varphi(r) = a\left(\frac{r-R_0}{t}\right)^2 + c, \quad (14b)$$

Exponential: $$E_\varphi(r) = \alpha\, Exp\left(n\frac{r-R_0}{t}\right), \quad (14c)$$

where r is the radial coordinate position, R_0 is the radius of the inner surface of the ring, t is the wall thickness; and α, n, m, a, b and $c$are coefficients to be fit with the experimental data.

Pilot simulations of a functionally graded ring showed that the circumferential strain profiles had the neutral axis shifted toward the external surface, compared to the neutral axis position of a homogeneous ring. This effect has been experimentally shown both in this study (Figure 7) and in edge bearing test results reported by Sharma et al. [10]. Therefore the neutral axis shift was used in the calibration process to determine the elastic modulus variation for each assumed distribution.

The fitting process began by selecting initial coefficients (α, n, m, a, b and c) for the fitting functions of Eq. 14. Then, a Matlab (Mathworks Inc) script was used to generate a table of elastic properties describing the gradation through the wall thickness. These properties were used in the FE ring model to which a loading curve in the linear elastic zone was applied. Displacements and the neutral axis positions from the FE model were compared with experimentally obtained results through an objective function F_t. The minimization function *fminsearch* (Matlab) was used to optimize these coefficients to reduce the error. The process was iterated upon until an acceptable error level of less than 4.5% was achieved. The target function F_t was defined as the sum of the normalized absolute deviations between the experimental (s_{exp}) and FE model (s_{FEM}) loading slopes, and the experimental (N_{exp}) and FE model (N_{FEM}) neutral axis positions in the east quadrant. The function was then defined as:

$$F_t = \frac{|s_{exp} - s_{FEM}|}{2|s_{exp}|} + \frac{|N_{exp} - N_{FEM}|}{2|N_{exp}|}, \quad (15)$$

in which each term was also divided by 2 in order to measure the average error with respect to the experimental values.

Overall, the three functions used to represent the gradation of the circumferential modulus provided a relatively good approximation of the strain fields as it was possible to reduce the error to below 4.5%in all cases (Table 2).

Table 2. Circumferential elastic distribution fitting parameters

Species	Specimen	Linear fit			Exponential fit			Parabolic fit		
		m	*b*	Error (%)	*α*	*n*	Error (%)	*a*	*c*	Error (%)
Moso	M-32	1578	878	4.5	1044	0.81	3.3	1417	1095	0.8
	M-14	1521	1171	0.3	1228	0.80	0.7	1331	1394	0.0
	Mean	1550	1025		1136	0.80		1374	1244	
Tre Gai	T-11	920	933	3.3	1027	0.56	3.7	872	1059	3.1
	T-102	809	882	0.3	927	0.60	0.3	1016	695	0.0
	Mean	864	908		977	0.58		944	877	
Guadua	G-24	990	559	0.0	609	0.96	0.2	836	704	0.4
	G-34	1061	542	0.3	601	1.01	0.1	1014	669	0.1
	Mean	1025	550		605	0.98		925	686	

In addition, for each of the inner and outer positions, the circumferential moduli were very similar for the three functions (Figure 10). However, there were important differences with species, following the same trend of the effective elastic moduli.

a.

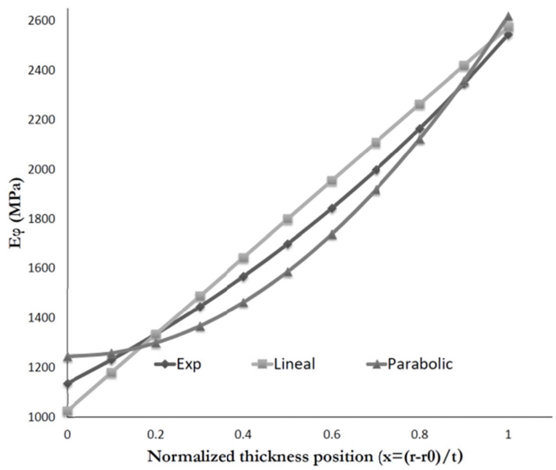

b.

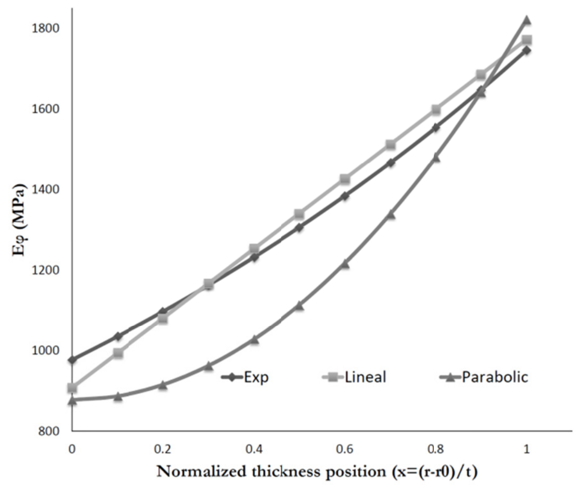

c.

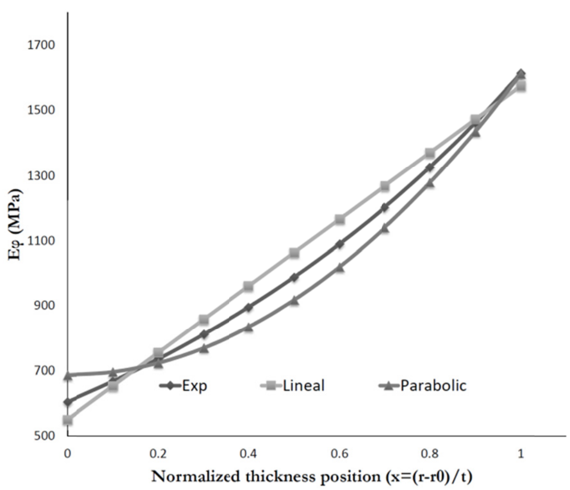

Figure 10. Circumferential modulus distributions obtained with the three functions for: a. Moso, b. Tre Gai, and c. Guadua.

Experimentally determined effective moduli (Table 1 and Figure 5) in Moso and Guaduafall beetween the average inner and outer moduli obtained with the fitted functions, while for Tre Gai, the effective modulus is lower than even the inner surface modulus

(Figure 11).The mean moduli at the outer position were 2.3, 1.9, 2.6 times higher than those at the inner location for Moso, Tre Gai, and Guadua, respectively.

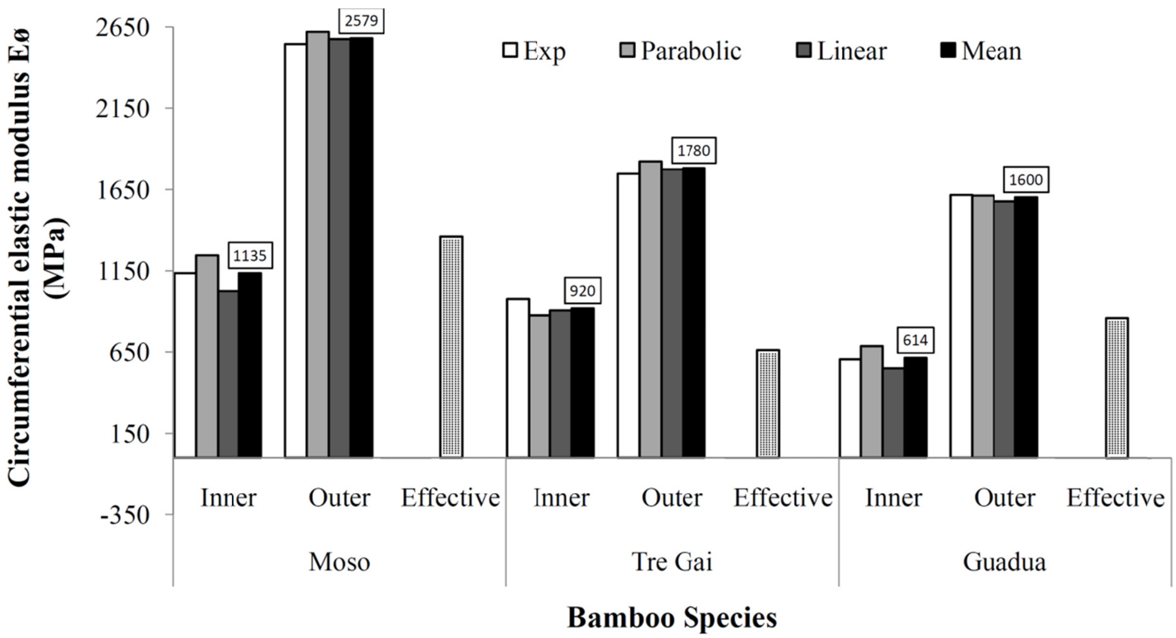

Figure 11. Summary of the circumferential moduli obtained in this study.

Similarly, the strain field obtained with the parabolic distribution in the FE models provided a relatively good approximation of the experimentally observed strains for Moso and Guadua, while, once again, the approximation was poor at the east location for Tre Gai (Figure 12).

There are a number of possible reasons for the poor modelling of Tre Gai, primarily the significant out-of-round asymmetry of the specimens (see Table 1 and Figure 9a). This considerable asymmetry caused substantial differences between East and West strain profiles (Figure 12b), which cannot be captured with the cylindrical shape assumed in the FE model.

a.

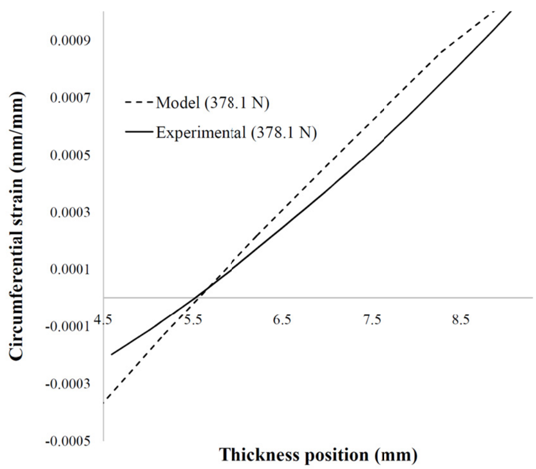

b.

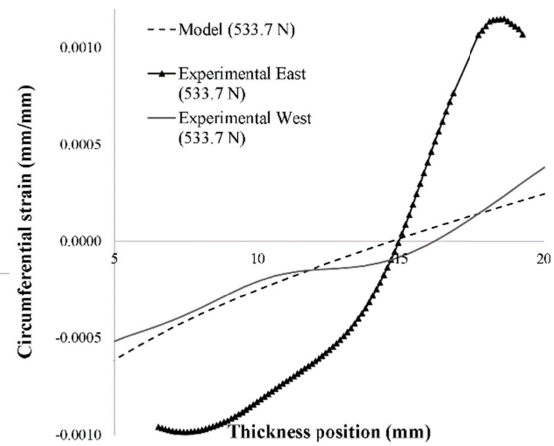

c.

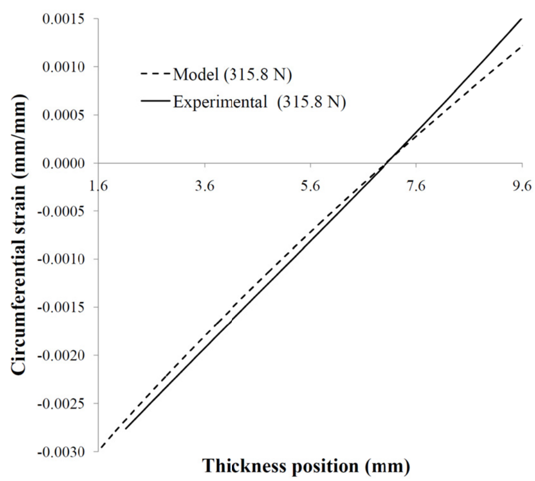

Figure 12. Circumferential strain profiles in compression test for bamboo specimens, a. M-14(East), b. T-11 (East and West) and c.G-34 (East)

3.5 Failure stresses

Failure stresses in the inner side of the rings were calculated as the product of mean inner circumferential moduli (Figure 11) and experimentally-determined maximum tension strains from the compression tests. They are equal to7.6 MPa (COV = 0.43), 12.1 MPa (COV = 0.26) and 3.7 MPa (COV = 0.38) for Moso, Tre Gai and Guadua, respectively.

4. DISCUSSION

An experimental study of the mechanical behavior of three commercially viable (for construction) bamboo species under circumferential loading was presented. Compression and tension edge bearing tests showed similar elastic effective moduli and neutral axis positions, which indicates that both tests are useful for the mechanical characterization of the transverse properties of bamboo. Digital image correlation analysis permitted an almost complete picture of strain profiles through the wall thickness in order to explain typical failures in tension and compression tests. Nonetheless, the compression test is significantly easier to conduct and is proposed to be promulgated in international standards, setting limits for the maximum variations of thickness and diameter of the specimens, in order to be consistent with the assumed circular geometry.

High ratios of outer and inner circumferential moduli predicted using all three assumed distribution functions (Eq. 14) are in agreement with the higher density of fibers near the outer boundary of the culm. This gradation should be taken into account in the analysis of bamboo elements for a more accurate estimation of the stress and strain distribution through the culm wall. Such advanced analyses will permit a better understanding of bamboo properties and be particularly useful in connection design. The circumferential gradation also explains the observed shift in the normalized position of the neutral axis (0.59-0.68) with respect to that estimated with a homogeneous model (0.53-0.59). This shift for Tre Gai bamboo falls within the range of 0.65 to 0.80 reported by Sharma [10].

As the effective elastic modulus depends on the position along the culm height [9, 17] and an exact provenance of the culms was not available, there is a wide scatter in the results. For instance, effective elastic moduli for the middle third of Guadua culms reported by Torres et al. [17] of 485 MPa is different from the average effective elastic modulus of 860 MPa reported here using the same protocol. On the other hand, average effective moduli for Moso and Tre Gai (1355 and 662 MPa) are also different from those reported by Sharma et al. [10] of 526 and 492 for Moso and Tre Gai respectively, and that reported by Torres et al.[17] for Moso of 1690 MPa. However, some specimens exhibited elastic modulus in the range reported by the aforementioned authors. This dispersion only demonstrates the natural variation that may be affects by such factors including, height along the culm, culm age and climate at harvest, and the nature of processing, treatment and storage prior to testing.

Jiang et al. [24] used uniaxial and biaxial compression edge bearing test and DIC to analyze the circumferential mechanical properties of bamboo rings of *Sinocalmus affinis*, however no strain values are provided and no discussion is made about the elastic modulus and its variation through the wall thickness. Other studies [10, 19] have reported strain profiles taking extreme values at the inner and outer face of the culm wall and assuming a linear behavior between these, which for thin wall bamboo rings appears to be a good approach. However for thick wall bamboo rings the strain profiles depicts substantial nonlinearities (Figures7 and 12).

Failure strains ranging from 5270 – 6270 $\mu\varepsilon$ on the inner surface reported by Lee et al. [19], and 1362-3011 $\mu\varepsilon$ reported by Sharma et al. [10] for the outer surface are near the experimental range reported in this study (1808-20412 $\mu\varepsilon$). In particular, the failure strains documented by Lee et al. for thin rings are similar to the mean values found in this study for the thin rings of Moso and Guadua, that were 6693 $\mu\varepsilon$ and 5948 $\mu\varepsilon$, respectively.

For the thin-walled Moso and Guadua, the circumferential elastic modulus variation was relatively well fitted with the three functions used. In a thin-walled ring, this is not surprising since the change in properties will not be terribly significant over a small thickness (see Figure 10). These functions showed differences among species, which suggest that these distributions are, nonetheless, species dependent. Results showed that Moso is the stiffer species followed for Tre Gai and Guadua.

The main limitation of this study was that the strain failures on the outer surface could not be measured due to the special device needed to accomplish the tension test. However, finite element models can be used to estimate these strains.

5. CONCLUSIONS

- A consistent behavior was observed between the tension and compression tests. Both, the effective elastic moduli and the observed shift of the neutral axis position, were similar in both tests. The compression test is recommended as it is simpler to be performed.
- Moso bamboo showed greater circumferential modulus than Tre Gai and Guadua.
- Loading curves and strain profiles permitted determining the transverse distribution of elastic modulus with reasonable precision using linear, exponential and parabolic distributions. All functions were able to simulate elastic distribution through the wall thickness of bamboo as other studies have shown. These elastic distributions showed being specie dependent.

- The normalized position of the neutral axis and tensile failure strain were similar in the thin wall bamboo species, Moso and Guada.
- DIC measurements allowed the determination of strain profiles in the critical positions and also helped to explain apparently anomalous test results.
- It is showed that in compression test, failures in quadrants different to North and South positions are due the presence of flaws in the material. Therefore, this type of failures should be discarded in field testing specimens.
- Variation in the circumferential elastic modulus through the thickness must be considered in the FE models of bamboo members for a more accurate prediction of their mechanical behavior.

ACKNOWLEDGEMENTS

The first author is grateful to Administrative Department of Science, Technology and Innovation COLCIENCIAS for financial support through national doctoral grant No. 617. All authors are thankful to The University of Pittsburgh for the use their laboratories and equipment and the Universidad del Valle for giving them the resources to undertake this study. The presented work was also supported by the US State Department IIE Global Innovation Institute (GII) award, which allowed for the collaboration between The University of Pittsburgh and Coventry University.

REFERENCES

[1] Ghavami K. and Culzoni R. Utilizaçao do Bambu como Material em Habitaçao de Baixo Custo. Simposio Internacional de Habitaçao, Sao Paulo; 1987.

[2] Laroque P. Design of a low cost bamboo footbridge. Master Engineering Thesis of Degree. Massachusets Institute of Technology; Massachusets, United States; 2007.

[3] Hidalgo O. Bamboo the gift of the gods. Bogotá, Colombia: Editorial D'Vinni; 2003.

[4] Ciro H., Osorio J., Vélez J. Determinación de la resistencia mecánica a tensión y cizalladura de la Guadua *angustifolia* Kunth. Revista de la Facultad de Ciencias Agropecuarias. Universidad Nacional de Medellín 2005; 58(1): 2709-2715.

[5] Janssen, J.J.A. Designing and building with bamboo. Technical report No. 20. International Network for Bamboo and Rattan; 2000.

[6] García J., Rangel C. and Ghavami K. Experiments with rings to determine the anisotropic elastic constants of bamboo. Construction and Building Materials 2012; 31: 52–57.

[7] Villegas L, Moran R, Garcia J. A new joint to assemble light structures of bamboo slats. Construction and Building Materials 2015; 98: 61–68

[8] Amada, S., Munekata, T., Nagase, Y., Ichikawa, Y., Kirigai A., and Zhifei, Y. Fiber texture and mechanical graded structure of bamboo. Composites: Part B 1997; 28B:13-20.

[9] Ghavami, K., Rodrigues, C. S. and Paciornik, S. Bamboo: functionally graded composite material. Asian journal of civil engineering (building and housing) 2003; 4 (1).

[10] Sharma B., Harries K., Ghavami K. Methods of determining transverse mechanical properties of full-culm bamboo, Constr. Build. Mater 2013; 38:627–637.

[11] Ghavami K, Moreira L. Development of a new joint for bamboo space structures. Transactions on the Built Environment 1996; 21.

[12] Moreira L, Ghavami K. Limits states analysis for bamboo pin connections. Key Engineering Materials 2012; 517: 3-12.

[13] Arce-Villalobos, O.A. Fundamentals of the design of bamboo structures. Doctoral Dissertation, *Eindhoven University of Technology*, Netherlands; 1993.

[14] López L., Correal J. Exploratory study of the glued laminated bamboo Guadua *angustifolia* as a structural material. Maderas. Ciencia Y Tecnología 2009; 11: 171–182.

[15] Ghavami, K., Marinho, A.B. Propriedades físicas e mecânicas do colmo inteiro do bambu da espécie Guadua angustifólia. Revista Brasileira de Engenharia Agrícola e Ambiental 2005; 9:107-114.

[16] Nogata and H. Takahashi. Intelligent functionally graded material: bamboo. Composites Engineering 1995; 5(7): 743-751.

[17] L.A. Torres, K. Ghavami, J.J. García, Determination of the circumferential Young's modulus of bamboo with diametric compression tests, Latin American Applied Research. 2007; 37: 255–260.

[18] Mitch, D., Harries, K.A., and Sharma, B. Characterization of Splitting Behavior of Bamboo Culms, *ASCE Journal of Materials in Civil Engineering*2010; 22(11): 1195-1199.

[19] Lee P., Odlin M., Yin H. Development of a hollow cylinder test for the elastic modulus distribution and the ultimate strength of bamboo. Construction and Building Materials 2014; 51: 235–243.

[20] Harries, K.A., Bumstead, J., Richard, M.J. and Trujillo, D. (in review) Geometric and Material Effects on Bamboo Buckling Behavior, *ICE Structures and Buildings* special issue on bamboo structures.

[21] Beer F, Jonhston E, Dewolf J, Mazurek D. Mechanic of materials. 6th ed. New York: McGraw-Hill; 2012.

[22] Young WC. Roark's formulas for Stress and Strain. 6th ed. New York: McGraw-Hill; 1989.

[23] Richard M., Harries K. On inherent bending in tension tests of bamboo. Wood Science Technology. Springer, 2014.

[24] Jian Z., Chen F., Wang G., Liu X., Shi S. and Cheng H. The circumferential mechanical properties of bamboo with uniaxial and biaxial compression tests. Bio Resources 7 (4) - 2012, pp. 4806-4816.